CICE2023 Rio de Janeiro – Brazil 11TH INTERNATIONAL CONFERENCE ON FRP COMPOSITES IN CIVIL ENGINEERING

Maintenance of all FRP pultruded structures. A Case study.

Ileana Ippolito[1] and Salvatore Russo[2]
Iuav University of Venice, Italy [1] iippolito@iuav.it [2] russo@iuav.it

ABSTRACT
FRP pultruded elements have seen limited use in construction for decades. Due to the need to rapidly built structures and retrofit or rehabilitate infrastructure, the use of fiber-reinforced materials in construction is implemented. The study focuses on an all FRP structures made by pultruded profiles characterized by maintenance and in situ check. It's a fundamental aspect to be taken into account in both design and verification phases for mechanical parts subjected in their service life to alternating or cyclic loads. The research analyzes maintenance process using also the AE monitoring technique. The conclusions recommend technical time frames regarding the monitoring and structural control of the nodes and the structure.

KEYWORDS
Maintenance; Oligocyclic test; Pultruded elements; Hollow profiles.

INTRODUCTION

The application of advanced composite materials in civil engineering has evolved slowly, mainly due to economic reasons. The main fields of application of the material concern three uses:
new constructions (pultruded FRP elements), reinforcement and rehabilitation of masonry structures, construction of hybrid structures made with the use of FRP in association with other building materials (Bedon and Louter, 2018)(Speranzini and Agnetti, 2015).The most common types of applications are mainly, hybrid concrete-FRP constructions (bridges, viaducts, etc.) and structural reinforcement of masonry structures (especially historic ones) for protection from seismic damage (Bank, 2006). These valuable innovations achieved with new materials demonstrate the good compatibility between FRP composites and brittle porous materials generally subjected to compressive stresses. FRP manufacturing technology has advanced in recent years (Xin, H. et al., 2017). In particular, the pultrusion process has been developed to produce continuous and long FRPs. Such FRPs have been shown to have excellent behavior to ultraviolet ray exposure, chemical corrosion, freeze-thaw cycle, dry-wet cycle, high temperature and humidity, are lightweight and high strength (Saleem et al, 2021). Thus, FRPs are widely used in the field of architecture, especially in recent years. According to the type of fiber, FRPs applied in civil engineering are often aramid-FRP, basalt-FRP, carbon-FRP and glass-FRP. Resin is often vinylester, epoxy and polyester (Naser et al., 2019). The world of fiber-reinforced polymers (FRPs) allows structural designers to achieve the goal of long-term sustainability in a wide range of applications; this is due not only to the mechanical properties of the materials, the reversibility and durability of the works, but also to the simplicity and rapidity of implementation for application (Boscato and Russo, 2013). Recently, in regions densely populated by earthquakes, advanced FRPs are increasingly being used for urgent retrofitting, rehabilitation, and strengthening of damaged structures due to increased ductility and strength especially in existing structures (Raza et al., 2020). Some exemples of FRP application are visible in the figure 1(Figure1).

a) **b)** **c)**

Figure 1 Examples of FRP structures, a) temporary walkway, b) post-earthquake coverage, c) Glass-House.

The greater the use of this material, the more its maintainability will have to be investigated, as various technical measures need to be taken to prolong its service life (Yumnam et al., 2021). Evaluation of material properties and monitoring by nondestructive techniques is extensively investigated within this article. Here, techniques for the maintenance and inspection of a frame made entirely of FRP with steel dry fasteners are reviewed. Acoustic emission tests and monitoring in its service life state were performed on the structure by subjecting it to continuous oligocyclic testing for the duration of 15 days.Special attention is given to connections between PFRP profiles and steel bolts (Mottram, 2004). These types of connections (currently not standardized) at the expense of bonding, have a good level of reversibility and non-invasiveness, as they are pointwise and the elements can be disassembled and reassembled very easily. The objective is to summarize the details of the techniques, equipment, and accuracy of these monitoring techniques.

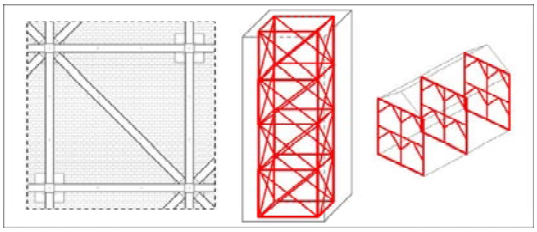

Figure 2 Type of reinforcement proposed.

STATE OF THE ART

From the studies carried out, as previously expressed, there appears to be a bibliographic gap on maintenance techniques on structures made entirely of FRP.

Specifically, the research, wants to try to relate two nondestructive monitoring techniques in order to identify the quality of the structure and develop possible maintenance interventions. The tests carried out within the laboratory used the combination of two techniques applicable during the state of service life of the structure (SLV):monitoring of the structure during low-frequency oligocyclic tests and monitoring of acoustic emissions (Ippolito and Russo, 2022).

Currently, standards referring to steel frames are especially used for setting FRP tests. Also in our case, the oligocyclic tests performed on the all-FRP structure were set using standards for testing steel structures, one at the European level and the other at the American level:

- *ECCS-45* European procedure of 1986 ("Recommended test procedure for evaluating the behavior of structural steel members under cyclic loads");
- *North-American ATC-24* (Applied Technology Council-24 "Guidelines for cyclic seismic testing of components of steel structures").

The European standard suggests how to structure a complete test. The test is structured in three tests, the first and second tests are applied together; they are performed by imposing on the specimen, monotonic displacements until failure, in order to evaluate the yield strength Fy^+ and the strain Ɛy^+ in one direction and in 'the other. The displacements are defined by the 'intersection of the tangent to the Fe curve at the origin, with the tangent to the Fe curve of slope 1/10th of the previous value (Figures 3). The third test is performed individually and subsequent to the first two; it consists of a cyclic test with increasing imposed displacement. Having calculated the yield displacement, 4 cycles are applied that have ¼ of the yield displacement as the value, and then groups of three cycles are applied that have (2+2n)Ɛy^+ and (2+2n)Ɛy^-, with n = 0,1,2,3.... Arriving at the collapse of the structure.

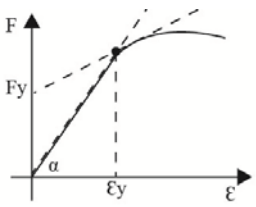

Figure 3 Experimental trial setting with the procedure of ECCS - 45.

The U.S. standard recommends applying increasing cycles of load, increasing them by a constant delta, until the structure collapses completely.

Most structural elements subjected to cyclic testing, involve single beam-column connections, a critical point in lightweight structures subjected to a cyclic action (McCrum *et al.*, 2019)(Hu *et al.*, 2020).
Acoustic emission (AE) monitoring is the main technology used to identify different types of failure in composite materials for in-service phase monitoring of the structure (C. R. Ramirez-Jimenez et al, 2004). Research on the acoustic response law of composites is useful to better understand the failure mechanisms and damage evolution of composites. The AE technique can also monitor damage and damage evolution in real time, both at the microscale and macroscale, evaluating the structural integrity of the components. AE can highlight fundamental damage mechanisms and fracture processes in composites. Damage mechanisms such as interfacial debonding of the matrix from the fiber, plastic deformation of the matrix, cracking, fiber tearing, and fiber fracture can be characterized by a variety of parameters referred to AE, especially the amplitude distribution (R. B. J. De Groot, Peter J., Peter AM Wijnen, 1995). Fast Fourier Transform (FFT) analysis is applied on the signals, which highlights the dominant frequencies directly related to the main fracture mechanism, while the Short-Time Fast Fourier Transform (ST-FFT) procedure provides the temporal information and thus the sequential events during the fracture process.

THE ALL FRP STRUCTURE

The structure is made completely of pultruded FRP box profiles and steel bolts. The elevated structure of the pavilion has a rectangular mesh size of 8500 mm x 1250 mm.
The C profile that characterizes the entire structure with a length of 8500 mm, is not a single profile, but is the result of the union of a beam with a length of 6000 mm and the other part with a length of 2500 mm.The vertical elements are box-shaped profiles made with 1250 mm x 4000 mm pultruded panels placed at a middle distance of 1250 mm. These panels are connected in foundation to a FRP stiffener structure fixed to a double support board with a total thickness of 80 mm (Figure 4).

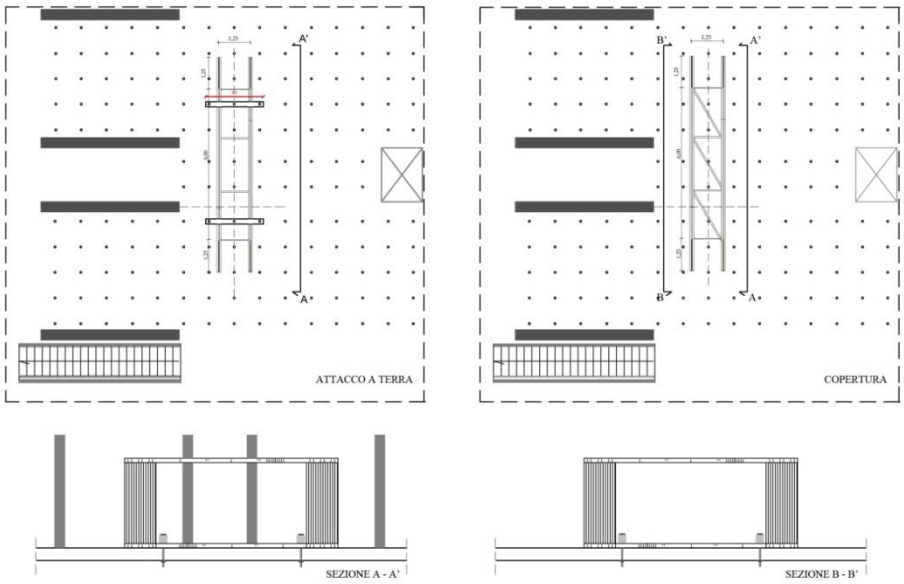

Figure 4 Pavilion, plan and prospects.

At floor level, the stiffener structure is made of two C profiles with dimensions 2000 mm x 600 mm x 100 mm fixed to the vertical panels. These profiles are the support surface of the paving slabs. To increase the stiffness orthogonal to the slabs, there are connections made up of 2 C profiles with dimensions of 2000mm x 600mm x 100mm near each slab between the portals. The roof also consists of two profiles C 2000mm x 600mm x 100mm similar to those indicated on the flooring, on which the pannels that have the function of covering are fixed. The bracing of the structure is made with angular profiles 1000mm x 1000mm x 80mm, fixed to the upper wings of the pavilion.
The pavilion was installed close to the actuator and a 0.10m thick wooden block was used for the connection between the two. It was chosen to apply the horizontal load of the actuator at the point of

discontinuity of the two main beams, the connection point between the two main beams, one of which is 6000mm long and the second 2500mm long (Figure 5).

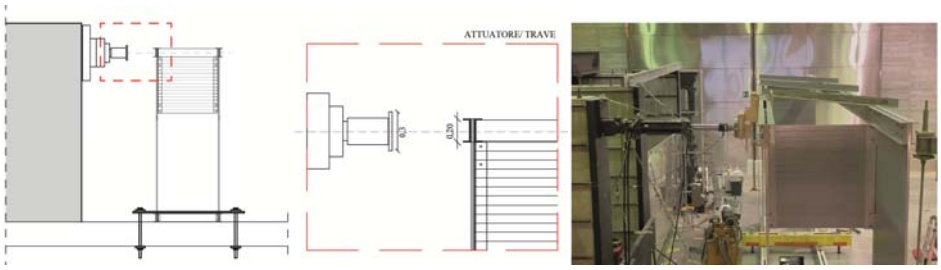

Figure 5 Placement of the actuator to the stressed node.

Set-up Test

Three different control systems were chosen for monitoring the structure:

- *Global monitoring*, actuator data reprocessing. The characteristics of the linear hydraulic actuator used is Model 201.35T with maximum capacity in compression: 365kN, maximum capacity in tension: 250Kn (Figures 6);
- *Local monitoring*, with the application of 3 transducers and a rotational control system [TR1-TR2-TR3]connected to an external data-return unit (Figures 7);
- *Spot monitoring*, carried out by the acoustic emission technique for dry latch testing using a controlled-tightening torque wrench, a 16-bit A/D converter on each channelto which a 19-mm-diameter stainless steel AE sensor with an operating frequency of 35-100 kHz, a peak sensitivity of 75 dB (Ref V/m/s) and a resonant frequency of 50 kHz was connected. The standards used to perform the tests were ISO 1996: 2-2017, DIN 45681:2005-03 and BS 4142: 2014. (Figure 8) (Ippolito and Russo, 2022).

Figure 6 Monitoring system used in testing.

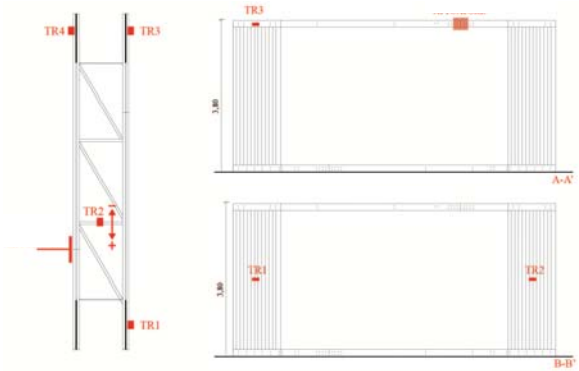

Figure 7 Pavilion plan with global control system.

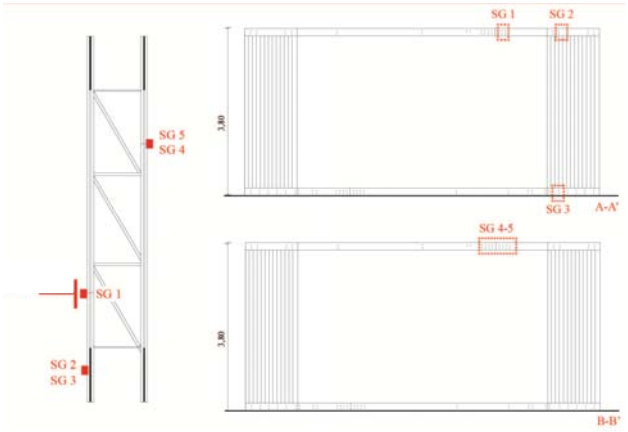

Figure 8 Pavilion plan with local control system.

Assuming that, the third part of the ECCS-45[1]procedure is used (εy^{+}) of the pavilion is applied as the yield displacement value (εy^{+}). From the pushover analysis the ultimate displacement of the pavilion was calculated at 1.43 = (εy^{+}).
Thus, a trilogy of cycles divided into macrogroups were defined:
4 cycles ⟶ ¼ Ɛy = ¼ 1.43 m = 0.35 m ≈ 350 mm
3 cycles ⟶ (2+2n)Ɛy = (2+2 · 1)1,43 m = 5,72 m ≈ 5 720 mm
3 cycles ⟶ (2+2n)Ɛy = (2+2 · 2)1,43 m = 8,52 m ≈ 8 520 mm

The values obtained by applying the norms, turn out to be greater than those we could apply on our structure, since the norms were designed to regulate tests to be carried out on frames made entirely of steel, unlike our structure which is a frame made of GFRP.
By comparing the results coming from the application of the regulations and the results obtained from the numerical model, we chose to work with displacements and frequencies that would allow us to maintain the structure in its working state, thus structuring a different test plan.
The tests had a total duration of 18 days, during which a load variation was applied on the pavilion such that the displacement was ±30mm for the first 15 days and ±50mm for the remaining 3 days (Table 1). The tests were carried out in continuity.

Table 1. Setting cyclic tests performed on the structure.

	Displacement (mm)	Frequency (Hz)	Time (day)	Number of cycles (1 day)
Test I	30	0.05	4	4 320
Test II	30	0.10	4	8 640
Test III	30	0.20	4	17 280
Test IV	30	0.40	3	34 560
Test V	50	0.40	3	34 560

AE monitoring was carried out in continuity with the test execution. The sensor recorded for the entire duration of the tests, and the collected data were later reprocessed with a data processing program and cleaned of background noise.

[1]ECCS-45 Recommended testing procedure for assessing the behaviour of structural steel elements under cyclic loads.

Low Cycle Fatigue (LCF)
Materials vary their response during the first cycles of plasticization in which there is greater movement of dislocations within the material. Because of this, at controlled stresses in strain the stress response of the material itself varies and two different behaviors can occur:
- *work hardening* (hardening), whereby the same strain becomes more and more onerous with each cycle;
- *softening* (softening), whereby the same strain becomes less and less onerous with each cycle.
In each case, the cyclic response tends to stabilize after a large number of cycles, and the resulting cycle, called the hysteresis cycle, is used to describe the stabilized cyclic response of the material. The cyclic response obtained is employed in the study of low-cycle fatigue, in which tests are usually conducted under total strain control, reporting the data in the form of a curve $\Delta \in = f(N)$. In a double logarithmic N - $\Delta\in$ plot, the experimental data tend to lie along two straight lines, showing independence between plastic strain terms and elastic strain terms (Figure 9).

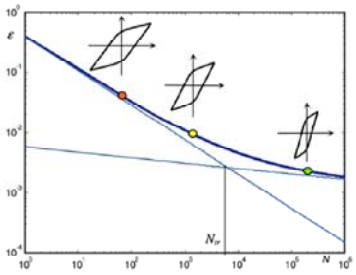

Figure 9 Diagram ∈-N

By dividing the total strain as the sum of the two components of which one part is elastic and one part is plastic, it is possible to write the following relationship for fatigue life N, Basquin's Relationship:

$$\frac{\Delta\epsilon_e}{2} = \frac{\Delta\sigma_a}{E} = \sigma'_f(2N)^b \qquad \text{Eq.1}$$

$$\frac{\Delta\epsilon_p}{2} = \epsilon'_f\ (2N)^c \qquad \text{Eq.2}$$

with b, c exponents of fatigue, σ'_f coefficient of fatigue strength, ϵ'_f coefficient of fatigue ductility.
By combining the previous relationships, the Coffin-Manson Relationship can be obtained:

$$\epsilon_a = \frac{\sigma'_f}{E}(2N)^b + \epsilon'_f(2N)^c \qquad \text{Eq.3}$$

To apply the Manson and Coffin equation and evaluate the number of cycles to failure, it is always necessary to calculate, as a result of the acting loads, the value of plastic Δε. This can be done experimentally, theoretically and numerically through the use of numerical modeling.

An alternative approach to classical prediction models (particularly the Coffin Manson model), is energy models for predicting the residual fatigue life of a material. In general, the fatigue criterion $\emptyset$ can be expressed as a generic function of the material stress state $\emptyset(\epsilon, \epsilon_p, \sigma, \Omega)$(S. Suresh, 1998) in the way that follows:

$$\emptyset\left(\epsilon, \epsilon_p, \sigma, \Omega\right)N^\beta = C \qquad \text{Eq.4}$$

where N is the fatigue life and β and C are typical material constants (in the case of the Coffin-Manson si ha ad esempio $\emptyset \equiv \Delta\epsilon_p$). Since physically the phenomenon of fatigue is associated from the microscopic point of view with the formation of micro defects, the movement of dislocations and all the phenomena that contribute to the nucleation of the fatigue crack, it seems natural to think of an energy criterion in order to quantify the presence of these micro defects. Based on Skelton's (Skelton,1991) considerations on the behavior in the plastic field of materials, concerning the phenomena of work hardening or softening, several authors (Constantinescu, 2021) have deepened and

investigated a predictive model for LCF based exclusively on the energy dissipated within the material during the hysteresis cycle. Writing the local energy equilibrium for a material gives:

$$\frac{dU}{dT} + \frac{dK}{dT} = \frac{dW}{dT} + \frac{dQ}{dT} \qquad \text{Eq.5}$$

with U internal energy, K kinetic energy, W mechanical work and Q heat produced.
Since K is negligible and Q can also be neglected under isothermal conditions (since mechanically dissipated heat is transmitted to the environment), it can be seen that the stored internal energy is only a function of mechanical work $\frac{dU}{dT} + \frac{dW}{dT}$.
For this reason, it has been proposed as a criterion for LCF:

$$\emptyset(x) = \int \sigma(x)\dot{\epsilon}(x)dt \qquad \text{Eq.6}$$

quantity that corresponds to the area enclosed by the hysteresis loop, the mechanical energy dissipated within the material. Specifically, the criterion becomes.

$$[\max \emptyset(x)]N^{\beta} = C \qquad \text{Eq.7}$$

if one considers that the stress-strain field is not uniform within the material. Values of β e C have to be determined experimentally, and their dependence, in addition to the material (composition and microstructure), on the temperature T at which fatigue tests are conducted, and on the stress ratio $R = \frac{\sigma_{max}}{\sigma_{min}}$ is debated in the literature and seems to be dependent on the materials analyzed. There are several cases of applications on steel structures in the literature, but the state of the art for polymer material structures is absent.

Failure analysis, closed formula and ae analyical approach
In order to determine the failure modes, the acoustic emission (AE) measurement method was used. The principle of this test is that the structure subjected to mechanical loading emits sound waves from the areas where physical changes have occurred, e.g., matrix deformation, fiber slippage, etc. If these sound waves are detected with a suitable microphone, the mode of failure can be determined based on the physical parameters of the waves (Figure 10).

Figure 10 Sound level meter and application of the instrument on the pavilion.

There is a significant relationship between crack initiation of brittle materials and energy release. Energy release is calculated from the induced voltage of each signal. The so-called AE energy is calculated by integrating the signal squared with the voltage. This signal is divided by 10 kOhm and then integrated by the duration of the AE waveform, as shown in equation (Eq.8).

$$E_{AE} = \sum \frac{V_S^2}{10(k\Omega)} \times 10^{-6}(sec) \times 1 \frac{\text{Joule}}{\text{Watt}-\text{sec}} \qquad \text{Eq.8}$$

For the test performed on boxed pultruded profiles, the value of E_AE is reported automatically through the MISTRAS system. This is indicated by a fast Fourier transform (FFT) on the event-related

waveform. To examine error modes based on the AE distribution, Khaple introduced a normalized amount of energy based on a fast Fourier transform (STFT) for the recorded AE signals. With this method, E (f) represents the energy ratio in frequencies and can be calculated as follows:

$$E(f) = \frac{\sum_{j=1}^{N} c(f_i,t_j)}{\sum_{i=1}^{M}\sum_{j=1}^{N} c(f_i,t_j)} \quad \text{Eq.9}$$

In this equation, C is the matrix of coefficients produced by STFT, t is time and f is frequency. In this equation, M and N are the number of discrete units in frequency and time, respectively. The normalized value E (f) is stated to be an important indicator of the energy components of the recorded signal. The value of E (f) is the ratio of the energy distributed in time to the energy distributed in both time and frequency. The E (f) introduced in equation (Eq.8) has J^(-1) as its unit.

To study the changing trend in the energy distribution in the frequency domain, the methodology introduced by Khaple was used. Note that E(f) is an energy ratio that considers the energy distribution in both time and frequency domains (Eq.8). The AE events resulting from the cracks produced a random energy distribution in the frequency domain, with the main energy peaks occurring before 140 Hz. The points used to survey the acoustic emissions were set with the objective of assessing any damage on the material during the conduct of the oligocyclic tests.

From these it can be inferred that the energy peaks occurred mainly at low frequencies (40 Hz) for all the data collected. It can be observed that the shape of the responses is similar to those reported in the literature (Kaphle, 2012) as mechanical cracks.

DISCUSSION

The graphs are the result of a testing campaign that lasted about 18 days. The tests took place continuously, returning a considerable amount of data.

It should also be noted that there are no oligocyclic tests on frames made entirely of FRP in the bibliography. Below are graphs regarding the return of the cyclic tests divided by frequency, highlighting the resulting differences among the 5 tests.

Test I: The graph below is the result of *Test I* (Table 1), lasting 4 days, during which the structure was stressed with a frequency of 0.05 Hz. The displacement throughout the duration of the test was controlled by the control unit system connected to the actuator and was imposed at 30 mm.

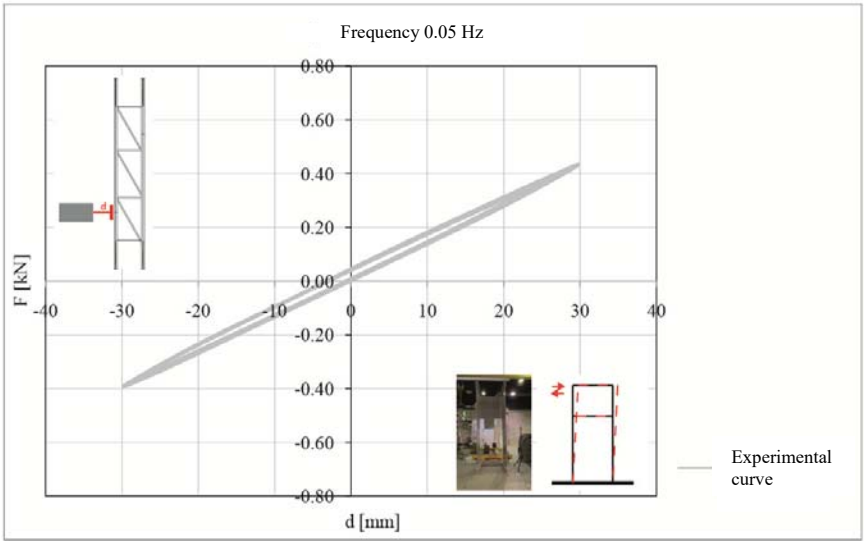

Figure 11 Load-Displacement Chart 0.05 Hz

The results demonstrate hysteresis loop behavior that stabilized following the first 3 hours of testing. The phenomenon of stabilization, takes the name of shakedown. From the deformation of the graphs, it is denoted that the linear elastic bond undergoes a translation, resulting in different hysteresis cycles depending on the imposed frequency. From the graph (Figure 10) it can be seen how the maximum strain tends to stabilize progressively with the number of cycles at constant load amplitude.

Test II: The graph below is the result of *Test II* (Table 1), lasting 4 days, during which the structure was stressed with a frequency of 0.10 Hz. The displacement throughout the duration of the test was controlled by the control unit system connected to the actuator and was imposed at 30 mm.

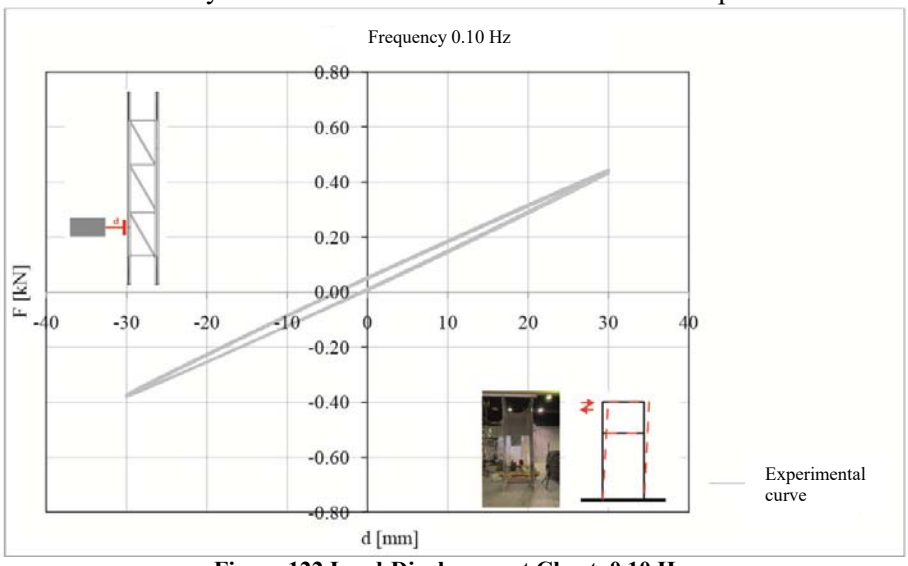

Figure 122 Load-Displacement Chart 0.10 Hz

The results represent the hysteresis cycles achieved by the structure in the 96-hour test. In contrast to Test I, the linear elastic bond undergoes a translation of ε_p (Figure 12). The hysteresis cycle denotes an area 6% greater than the test performed with the frequency at 0.05 Hz.

Test III: The graph below is the result of Test III (Table 1), lasting 4 days, during which the structure was stressed with a frequency of 0.20 Hz. The displacement throughout the duration of the test was controlled by the control unit system connected to the actuator and was imposed at 30 mm.

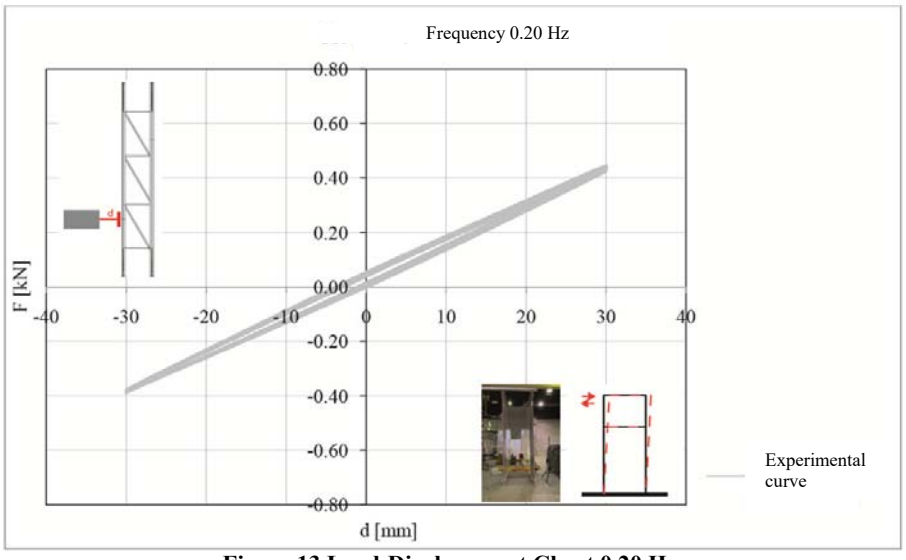

Figure 13 Load-Displacement Chart 0.20 Hz

The results represent the hysteresis cycles achieved by the structure over the 96-hour test period. The bond undergoes a translation of ε_p, reducing by 2% (Figure 13).

Test VI: The graph below is the result of the VI Test (Table 1), lasting 3 days, during which the structure was stressed with a frequency of 0.40 Hz. The displacement throughout the duration of the test was controlled by the control unit system connected to the actuator and was imposed at 30 mm.

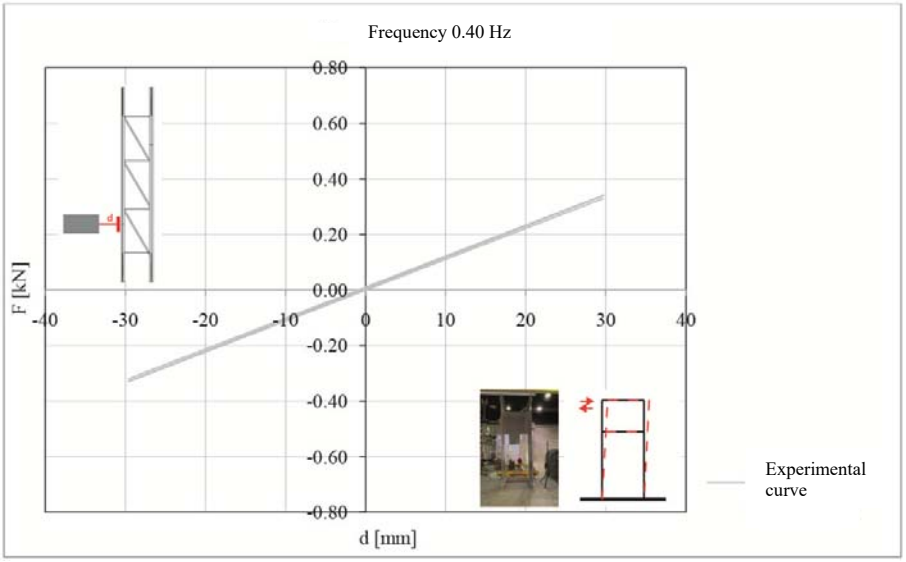

Figure 14 Load-Displacement Chart 0.40 Hz

The results represent the hysteresis cycles achieved by the structure over the 72-hour test period. Unlike the tests with lower frequencies, it can be seen from the graph (Figure 14) that the structure has a hysteresis cycle that tends to zero. During this phenomenon, the tension-strain cycle tends to overlap and remain stable. This phenomenon along with the phenomenon of accommodation are effects of the deformation cycles in the plastic field.

Test V: The graph below is the result of Test V (Table 1), lasting 3 days, during which the structure was stressed with a frequency of 0.40 Hz. The displacement for the duration of the test was controlled by the control unit system connected to the actuator and was imposed at 50 mm. For the last test, we wanted to increase both the distance and the frequency in order to study the behavior of the structure in a critical situation.

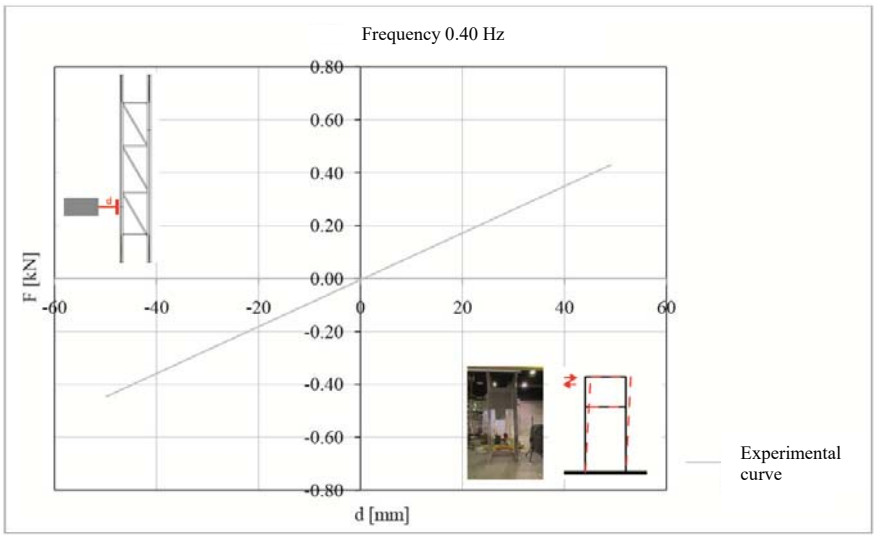

Figure 15 Load-Displacement Chart 0.40 Hz

The results represent the hysteresis cycles achieved by the structure over the 72 hours of testing. In contrast to the tests with lower frequencies, in Figure 15, it can be seen that the structure stabilized, creating a hysteresis cycle is that traceable to a straight line. During this phenomenon, the tension-strain cycle tends to overlap and remain stable.

During the tests, acoustic monitoring was carried out through sound emission recordings by applying the accelerometer as visible from the figure (Figure 8). The results of the recordings during the 5 tests can be seen from the summary graph below (Figure 16).

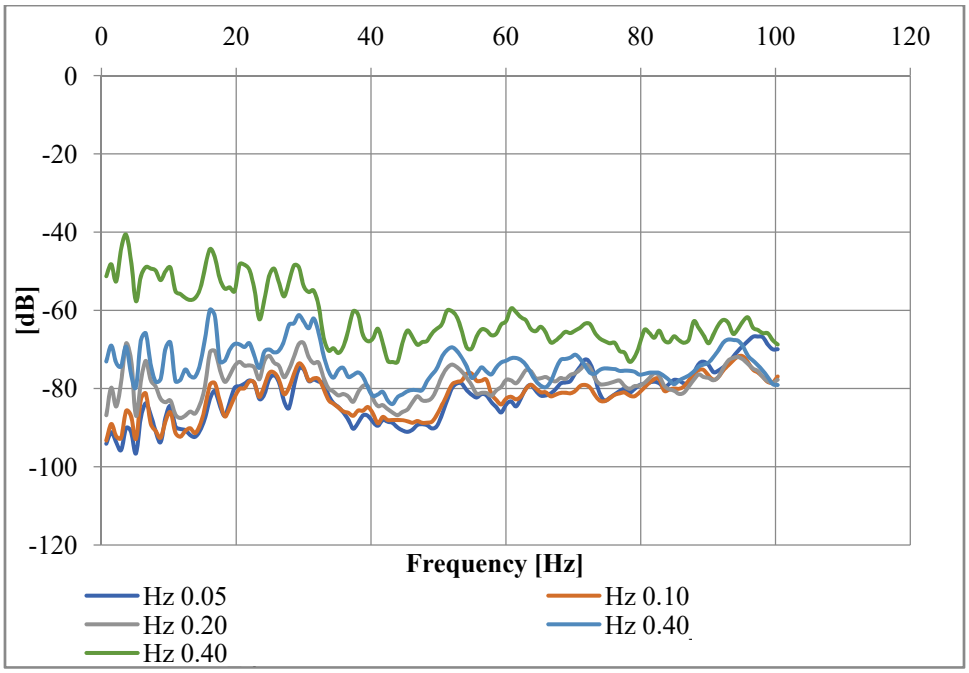

Figure 16 Trend of acoustic emission during tests

The analysis of noise emissions, reported that at high frequencies (between 0/20 Hz), the curves for the recordings that occurred during the 96-hour test (for the cycles performed at 0.05 Hz and 0.10 Hz) are between -97 dB and -78 dB. For the test performed up to 0.20 Hz, the recorded emissions are between -80 dB and -60 dB. It follows that as the frequencies imposed on the structure increase, there appears to be an increase in acoustic emission.

CONCLUSION

The tests conducted in order to identify a maintenance methodology for structures refer to the oligocyclic behavior of a construction made with an all FRP frame.

The following can also be deduced from the tests:

- Applying the equation for calculating the area of the hysteresis loop (Eq.7), during the test carried out with an imposed frequency of 0.10 Hz, it was found that the area has a size 6% larger than the area resulting from the hysteresis loop of the test with a frequency of 0.05 Hz, and 8% larger than the test carried out with a frequency of 0.20 Hz;
- Punctual monitoring of the structure with strain gauges, allowed the reading of material deformation along the direction of the fibers. In the test carried out with an imposed frequency of 0.05 Hz, the strain increase was 20% with a strain increase from 0.05 Hz to 0.06 Hz. For the test carried out at frequency 0.20 Hz, there was a strain increase of 8%, with an increase in strain from 0.20 Hz to 0.22 Hz. During the test performed with an imposed frequency of 0.40 Hz, a fiber strain of 13% was recorded from 0.40 Hz to 0.45 Hz, after 60 hours from the start of the test;
- From the analysis of the acoustic emissions, it was found that at high frequencies (between 0/20 Hz), the curves for the recordings that occurred during the 96-hour test (for the cycles performed at 0.05 Hz and 0.10 Hz) ranged from -97 dB to -78 dB. For the test performed up to 0.20 Hz, the recorded emissions are between -80 dB and -60 dB. It follows that as the frequencies imposed on the structure increase, there appears to be an increase in acoustic emission.

Maintenance of an FRP structure that is placed in a low seismicity zone is recommended at least every 365 days. Comparing the tests that occurred in the laboratory with other tests that occurred on the structure in use, the ceck of the bolts recorded a 10% loss on the roof, following 11 months of use of the roof . The testing of the fasteners on the ground attachment recorded no leakage. As a result of the testing campaign conducted on the structure, it follows that checking the fasteners is recommended on a semi-annual basis.

No deterioration of the material at the aesthetic level was detected, as no color changes or damage was reported at the macroscopic level.

References

Constantinescu, A., Charkaluk, E., Lederer, G., & Verger, L. (2004). A computational approach to thermomechanical fatigue. International Journal of fatigue, 26(8), 805-818.

Bank, L. C. (2006). Composites for construction: structural design with FRP materials. John Wiley & Sons.

Bedon, C., & Louter, C. (2017). Numerical analysis of glass-FRP post-tensioned beams–Review and assessment. *Composite Structures*, *177*, 129-140.

McCrum, D. P., Simon, J., Grimes, M., Broderick, B. M., Lim, J. B., & Wrzesien, A. M. (2019). Experimental cyclic performance of cold-formed steel bolted moment resisting frames. *Engineering Structures*, *181*, 1-14.

Mottram, J. T. (2004). Shear modulus of standard pultruded fiber reinforced plastic material. *Journal of Composites for Construction*, *8*(2), 141-147.

Naser, M. Z., Hawileh, R. A., & Abdalla, J. A. (2019). Fiber-reinforced polymer composites in strengthening reinforced concrete structures: A critical review. *Engineering Structures*, *198*, 109542.

Hu, W., Li, Y., & Yuan, H. (2020). Review of experimental studies on application of FRP for strengthening of bridge structures. *Advances in Materials Science and Engineering*, *2020*, 1-21.

Hu, Y., Zhao, J., Zhang, D., & Zhang, H. (2020). Cyclic tests of fully prefabricated concrete-filled double-skin steel tube/moment-resisting frames with beam-only-connected steel plate shear walls. *Thin-Walled Structures*, *146*, 106272.

Yumnam, M., Gupta, H., Ghosh, D., & Jaganathan, J. (2021). Inspection of concrete structures externally reinforced with FRP composites using active infrared thermography: A review. *Construction and Building Materials*, *310*, 125265.

Ippolito, I., & Russo, S. (2022). Maintenance and Structural Check of an All FRP Pultruded Construction. In *10th International Conference on FRP Composites in Civil Engineering: Proceedings of CICE 2020/2021 10* (pp. 131-142). Springer International Publishing.

Raza, A., Khan, Q. U. Z., & Ahmad, A. (2020). Prediction of axial compressive strength for FRP-confined concrete compression members. *KSCE Journal of Civil Engineering*, *24*(7), 2099-2109.

Saleem, M. A., Zafar, M. N., Saleem, M. M., & Xia, J. (2021). Recent developments in the prefabricated bridge deck systems. *Case Studies in Construction Materials*, *15*, e00750.

Santarsiero, M., Bedon, C., & Louter, C. (2018). Experimental and numerical analysis of thick embedded laminated glass connections. *Composite Structures*, *188*, 242-256.

Speranzini, E., and S. Agnetti. "Flexural performance of hybrid beams made of glass and pultruded GFRP." Construction and Building Materials 94 (2015): 249-262.

Suresh, S. (1998). *Fatigue of materials*. Cambridge university press.

Skelton, R. P. (1991). Energy criterion for high temperature low cycle fatigue failure. Materials science and technology, 7(5), 427-440.

Xin, H., Liu, Y., Mosallam, A. S., He, J., & Du, A. (2017). Evaluation on material behaviors of pultruded glass fiber reinforced polymer (GFRP) laminates. Composite Structures, 182, 283-300.

The authors declare that they have no conflicts of interest associated with the work presented in this paper.

Data on which this paper is based is available from the authors upon reasonable request.